Supplementary Information: "Freshwater transport from warm to cold ocean regions amplifying faster than all model estimates"

Taimoor Sohail[1], Jan D. Zika[1], Damien B. Irving[2], and John A. Church[3]

[1]School of Mathematics and Statistics, University of New South Wales, Sydney, Australia
[2]Commonwealth Scientific and Industrial Research Organisation (CSIRO), Hobart, Australia
[3]Climate Change Research Centre, University of New South Wales, Sydney, Australia

July 16, 2021

1 Time-mean T–S curve and surface freshwater fluxes

Understanding the change in freshwater content in the global ocean requires an understanding of the time-mean climatological state of the ocean, shown in figure S1. The T–S curve in figure S1a shows that, generally, the tropical and sub-polar oceans are characterised by relatively fresh water, and the sub-tropics are characterised by relatively salty water. This clear distinction between climatological regions is driven in part by surface water fluxes which, on average, dump freshwater into the tropics and sub-polar regions via precipitation and river runoff and draw freshwater from the sub-tropics via evaporation (figure S1b). In a 'wet-gets-wetter-dry-gets-drier' world, the T–S curve would move to the right in the sub-tropics and to the left in the tropics and sub-polar oceans, with the T–S extrema moving further apart. While the CMIP6 models recreate the shape of the T–S curve seen in the observations, the majority are biased fresh compared to the observations. This difference may be due to the fact that the CMIP6 mean T–S curve is calculated based on a pre-industrial control run (prior to 1850), while the observational mean T–S curve is calculated based on an average from 1970 to 2014. The surface freshwater flux (integrated from hot to cold) shows that the CMIP6 ensemble-mean and observations roughly align in warmer temperature-percentiles. However, there is a relative lack of agreement between observations and CMIP6 models in colder temperature-percentiles. The observational data set does not include the contribution of sea ice (peak in freshening at coldest temperature-percentiles in the CMIP6 models), and thus disagrees with CMIP6 at the coldest percentiles.

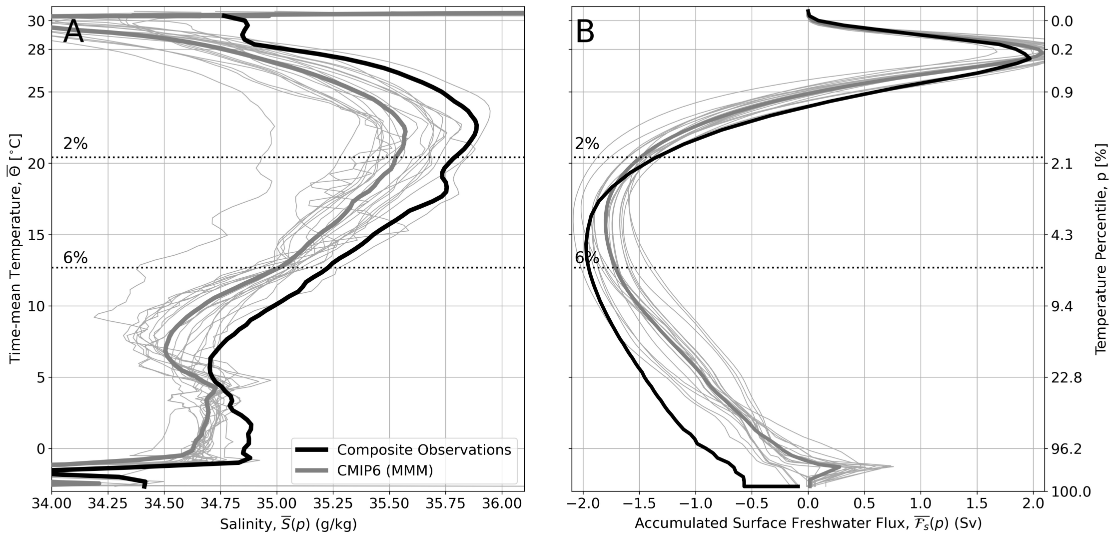

Figure S1: Global a) T–S curve averaged from 1970 to 2014 in the observations and over the pre-industrial control period in the CMIP6 models, and b) surface freshwater fluxes $\mathcal{F}_s$, averaged over the 1979-2011 period in the observations and over the pre-industrial control period in the CMIP6 models. Light grey lines represent each CMIP6 model member, and thick grey line represents the CMIP6 multi-model mean (MMM). The right-hand y-axis shows the corresponding accumulated temperature-percentile in observations, and horizontal dotted lines indicate the warmest 2% and warmest 6% of the ocean by volume.

2 T–S Changes

As shown in figure 2, we track changes in the ocean's T–S curve in the observations and CMIP6 multi-model mean to understand changes in salinity over the past fifty years. Here we present changes in the T–S curve in the DAMIP GHG-only, AA-only and corresponding CMIP6 historical runs, shown in figure S2b, c and d, respectively. The multi-model mean T–S change in the six CMIP6 historical runs corresponding to the DAMIP models is similar to the multi-model mean change for all CMIP6 models in figure 2b. The GHG-only multi-model mean T–S change exhibits a larger magnitude of salinification to the all forcing ensemble-mean over a similarly narrow band of temperature-percentiles, between the warmest ∼0.2% and 2% of the ocean. AAs, on the other hand, drive an opposite trend in water cycle change, with the sub-tropics getting fresher and the rest of the ocean salinifying. The freshening signal in the sub-tropics in the AA-only mean is roughly of equal and opposite magnitude to the salinification signal in the observations, over a similar range of temperature-percentiles.

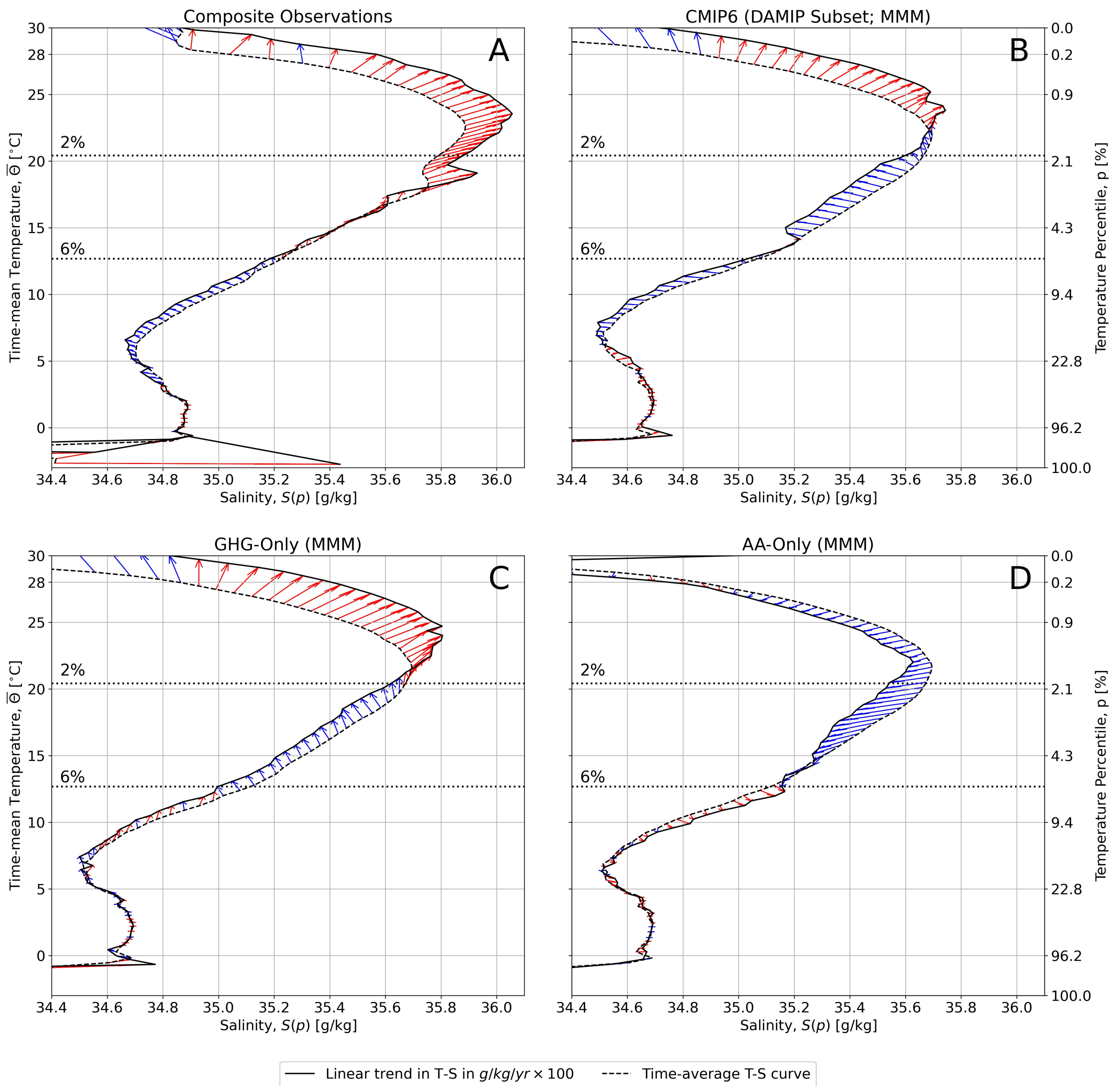

Figure S2: Linear trend in the global T–S curve, in $g/kg/yr \times 100$, in a) observations, b) the DAMIP all forcing, c) GHG-only and Aerosol-only multi-model means (MMM). Arrow vectors are coloured by the sign of the salinity change, red implying salinification and blue implying freshening. The right-hand y-axis shows the corresponding accumulated temperature-percentile in observations.

3 Freshwater Flux Changes

While figures 3 and 4 focus on freshwater fluxes and surface freshwater fluxes in the warmest 2% and warmest 6% of the ocean, in figure S3 we present freshwater fluxes for all percentiles, integrated from hot (0%) to cold (100%). As these plots are integrated from hot to cold, the sign of the slope of the lines indicates a freshening or salinification. The observations and CMIP6 models freshen in the warmest ∼0.2% of the ocean, before salinifying in the warmest 6% and 2% of the ocean, respectively (see figure S3a). This salinification has been discussed at length in the main text of the manuscript. In the warmest ∼22.8% of the ocean, the CMIP6 models experience a strong peak in freshening, which is not replicated in the observations. To explore the extent to which the global freshwater fluxes are modulated by surface freshwater fluxes, we visualise the integrated surface freshwater fluxes in the observations and CMIP6 mean in figure S3b. There is an increase in precipitation over the warmest 0.2% of the ocean, followed by net increase in evaporation (relative to precipitation and river runoff) over a narrow band of temperature-percentiles. The range of temperature-percentiles that experience an intensification of evaporation does not align with the broader range of percentiles over which salinification occurs in the CMIP6 mean. Therefore, there is some component of circulation and mixing changes that impacts the salinification in the global freshwater fluxes in panel S3a. In addition, the surface freshwater fluxes show a net evaporation over the warmest ∼22.8% of the ocean, despite the global freshening in this volume shown in panel S3a. Therefore, we posit that the peak freshening seen here is a consequence of changes in ocean circulation and mixing, possibly due to changes in high-latitude ocean ventilation.

Figure S3c and d show the global and surface freshwater flux changes in the observations, CMIP6 mean, and the DAMIP runs. GHG-forced DAMIP models show a stronger salinification up to the warmest 2% of the ocean compared to the corresponding CMIP6 historical runs (compare red/orange lines with purple/magenta lines in figure S3c). In addition, the strong freshening between the warmest 2% and warmest ∼22.8% of the ocean in the CMIP6 historical runs is not replicated in a GHG-only simulation, with little freshwater change in these layers. AA-only simulations instead show a strong freshening in the warmest 6% of the ocean (blue/light blue lines in figure S3c). The GHGs and AAs in the climate models interact in a complex manner to yield the CMIP6 historical response - a weak salinification in the warmest 2% of the ocean and strong freshening in the warmest ∼22.8% of the ocean (purple/magenta lines in figure S3c).

The stark difference in global freshwater fluxes in the GHG-only and AA-only runs may be explained, in part, by the surface flux tendencies in figure S3d. The stronger freshening and salinification in the warmest 2% ocean in the GHG-only runs may, in part, be attributed to stronger increased net precipitation and evaporation in the surface freshwater fluxes in figure S3d. In addition, the GHG-only runs experience similar net evaporation over the warmest ∼22.8% of the ocean compared with the all-forcing runs, but do not experience the same peak in freshening as in the corresponding CMIP6 historical runs. We propose that the strong evaporation in the GHG-only runs at warmer percentiles and/or circulation changes may explain the lack of a freshening peak in the GHG-only runs. The AA-only runs show broadly the opposite trend in surface freshwater flux tendencies to the GHG-only and all-forcing runs.

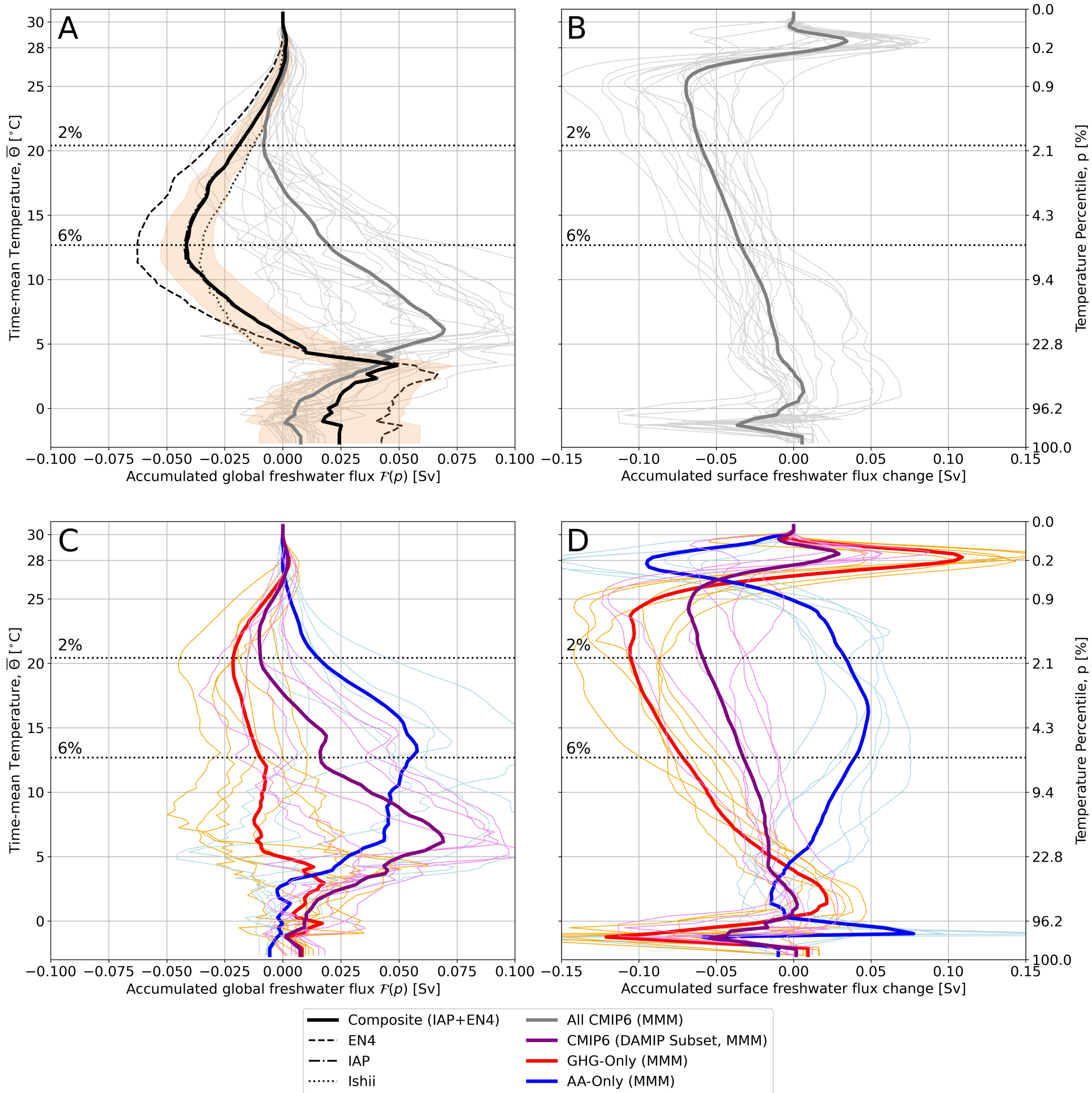

Figure S3: a) The global freshwater accumulation rate, integrated from hot to cold, inferred from the salinity tendency in observations and the CMIP6 models. b) The surface freshwater flux change, integrated from hot to cold, in the CMIP6 models. c) The global freshwater accumulation rate, integrated from hot to cold, inferred from the salinity tendency in the DAMIP models and corresponding CMIP6 historical runs. d) The surface freshwater flux change, integrated from hot to cold, in the DAMIP model and corresponding CMIP6 historical runs. Orange shading in a) shows the standard error of the slope of the linear regression over time. The right-hand y-axis shows the corresponding temperature-percentile in the observational dataset. Horizontal dotted lines indicate the warmest 2% and warmest 6% of the ocean.

4 Summary of CMIP6 and DAMIP models

Table S1 summarises the CMIP6 models and ensemble members used in this study. Only the first ensemble member was used from each model.

Table S2 summarises the DAMIP models and ensemble members used in this study.

	Model Name	Ensemble Member	Group	Data Citations
1	ACCESS-CM2	r1i1p1f1	Salty	[30]
2	ACCESS-ESM1-5	r1i1p1f1	Salty	[31]
3	CanESM5	r1i1p1f1	Fresh	[32]
4	CanESM5-CanOE	r1i1p2f1	Fresh	[33]
5	CMCC-CM2-SR5	r1i1p1f1	Salty	[34]
6	CNRM-CM6-1	r1i1p1f2	Fresh	[35]
7	CNRM-ESM2-1	r1i1p1f2	Fresh	[36]
8	EC-Earth3	r1i1p1f1	Salty	[37]
9	EC-Earth3-Veg	r1i1p1f1	Fresh	[38]
10	EC-Earth3-Veg-LR	r1i1p1f1	Fresh	[39]
11	FGOALS-f3-L	r1i1p1f1	Fresh	[40]
12	HadGEM3-GC31-LL	r1i1p1f3	Fresh	[41]
13	IPSL-CM6A-LR	r1i1p1f1	Salty	[42]
14	MIROC-ES2L	r1i1p1f2	Salty	[43]
15	MPI-ESM-1-2-HAM	r1i1p1f1	Salty	[44]
16	MPI-ESM1-2-HR	r1i1p1f1	Salty	[45]
17	MPI-ESM1-2-LR	r1i1p1f1	Salty	[46]
18	NorESM2-LM	r1i1p1f1	Fresh	[47]
19	NorESM2-MM	r1i1p1f1	Salty	[48]
20	UKESM1-0-LL	r1i1p1f2	Fresh	[49]

Table S1: Suite of CMIP6 models used in this study.

	Model Name	Ensemble Member	Data Citations
1	ACCESS-CM2	r1i1p1f1	[50]
2	ACCESS-ESM1-5	r1i1p1f1	[51]
3	CanESM5	r1i1p1f1	[52]
4	CNRM-CM6-1	r1i1p1f2	[53]
5	HadGEM3-GC31-LL	r1i1p1f3	[54]
6	IPSL-CM6A-LR	r9i1p1f1	[55]

Table S2: Suite of DAMIP models used in this study.

References

[30] Martin Dix, Doahua Bi, Peter Dobrohotoff, Russell Fiedler, Ian Harman, Rachel Law, Chloe Mackallah, Simon Marsland, Siobhan O'Farrell, Harun Rashid, Jhan Srbinovsky, Arnold Sullivan, Claire Trenham, Peter Vohralik, Ian Watterson, Gareth Williams, Matthew Woodhouse, Roger Bodman, Fabio Boeira Dias, Catia Domingues, Nicholas Hannah, Aidan Heerdegen, Abhishek Savita, Scott Wales, Chris Allen, Kelsey Druken, Ben Evans, Clare Richards, Syazwan Mohamed Ridzwan, Dale Roberts, Jon Smillie, Kate Snow, Marshall Ward, and Rui Yang. CSIRO-ARCCSS ACCESS-CM2 model output prepared for CMIP6 CMIP. *Earth System Grid Federation*, 2019. Version 20191108.

[31] Tilo Ziehn, Matthew Chamberlain, Andrew Lenton, Rachel Law, Roger Bodman, Martin Dix, Yingping Wang, Peter Dobrohotoff, Jhan Srbinovsky, Lauren Stevens, Peter Vohralik, Chloe Mackallah, Arnold Sullivan, Siobhan O'Farrell, and Kelsey Druken. CSIRO ACCESS-ESM1.5 model output prepared for CMIP6 CMIP. *Earth System Grid Federation*, 2019. Version 20191214.

[32] Neil Cameron Swart, Jason N.S. Cole, Viatcheslav V. Kharin, Mike Lazare, John F. Scinocca, Nathan P. Gillett, James Anstey, Vivek Arora, James R. Christian, Yanjun Jiao, Warren G. Lee, Fouad Majaess, Oleg A. Saenko, Christian Seiler, Clint Seinen, Andrew Shao, Larry Solheim, Knut von Salzen, Duo Yang, Barbara Winter, and Michael Sigmond. CCCma CanESM5 model output prepared for CMIP6 CMIP. *Earth System Grid Federation*, 2019. Version 20190429.

[33] Neil Cameron Swart, Jason N.S. Cole, Viatcheslav V. Kharin, Mike Lazare, John F. Scinocca, Nathan P. Gillett, James Anstey, Vivek Arora, James R. Christian, Yanjun Jiao, Warren G. Lee, Fouad Majaess, Oleg A. Saenko, Christian Seiler, Clint Seinen, Andrew Shao, Larry Solheim, Knut von Salzen, Duo Yang, Barbara Winter, and Michael Sigmond. CCCma CanESM5-CanOE model output prepared for CMIP6 CMIP. *Earth System Grid Federation*, 2019. Version 20190429.

[34] Tomas Lovato and Daniele Peano. CMCC CMCC-CM2-SR5 model output prepared for CMIP6 CMIP. *Earth System Grid Federation*, 2020.

[35] Aurore Voldoire. CNRM-CERFACS CNRM-CM6-1 model output prepared for CMIP6 CMIP. *Earth System Grid Federation*, 2018. Version 20180917.

[36] Roland Seferian. CNRM-CERFACS CNRM-ESM2-1 model output prepared for CMIP6 CMIP. *Earth System Grid Federation*, 2018. Version 20181206.

[37] EC-Earth. EC-Earth-Consortium EC-Earth3 model output prepared for CMIP6 CMIP. *Earth System Grid Federation*, 2019. Version 20200310.

[38] EC-Earth. EC-Earth-Consortium EC-Earth3-Veg model output prepared for CMIP6 CMIP. *Earth System Grid Federation*, 2019. Version 20200225.

[39] EC-Earth. EC-Earth-Consortium EC-Earth3-Veg-LR model output prepared for CMIP6 CMIP. *Earth System Grid Federation*, 2020.

[40] Yongqiang Yu. CAS FGOALS-f3-L model output prepared for CMIP6 CMIP. *Earth System Grid Federation*, 2018.

[41] Jeff Ridley, Matthew Menary, Till Kuhlbrodt, Martin Andrews, and Tim Andrews. MOHC HadGEM3-GC31-LL model output prepared for CMIP6 CMIP. *Earth System Grid Federation*, 2018. Version 20190628.

[42] Olivier Boucher, Sébastien Denvil, Guillaume Levavasseur, Anne Cozic, Arnaud Caubel, Maire-Alice Foujols, Yann Meurdesoif, Particia Cadule, Marion Devilliers, Josefine Ghattas, Nicolas Lebas, Thibaut Lurton, Lidia Mellul, Ionela Musat, Juliette Mignot, and Frédérique Cheruy. IPSL IPSL-CM6A-LR model output prepared for CMIP6 CMIP. *Earth System Grid Federation*, 2018. Version 20180803.

[43] Tomohiro Hajima, Manabu Abe, Osamu Arakawa, Tatsuo Suzuki, Yoshiki Komuro, Tomoo Ogura, Koji Ogochi, Michio Watanabe, Akitomo Yamamoto, Hiroaki Tatebe, Maki A. Noguchi, Rumi Ohgaito, Akinori Ito, Dai Yamazaki, Akihiko Ito, Kumiko Takata, Shingo Watanabe, Michio Kawamiya, and Kaoru Tachiiri. MIROC MIROC-ES2L model output prepared for CMIP6 CMIP. *Earth System Grid Federation*, 2019.

[44] David Neubauer, Sylvaine Ferrachat, Colombe Siegenthaler-Le Drian, Jens Stoll, Doris Sylvia Folini, Ina Tegen, Karl-Hermann Wieners, Thorsten Mauritsen, Irene Stemmler, Stefan Barthel, Isabelle Bey, Nikos Daskalakis, Bernd Heinold, Harri Kokkola, Daniel Partridge, Sebastian Rast, Hauke Schmidt, Nick Schutgens, Tanja Stanelle, Philip Stier, Duncan Watson-Parris, and Ulrike Lohmann. HAMMOZ-Consortium MPI-ESM1.2-HAM model output prepared for CMIP6 CMIP. *Earth System Grid Federation*, 2019. Version 20190627.

[45] Johann Jungclaus, Matthias Bittner, Karl-Hermann Wieners, Fabian Wachsmann, Martin Schupfner, Stephanie Legutke, Marco Giorgetta, Christian Reick, Veronika Gayler, Helmuth Haak, Philipp de Vrese, Thomas Raddatz, Monika Esch, Thorsten Mauritsen, Jin-Song von Storch, Jörg Behrens, Victor Brovkin, Martin Claussen, Traute Crueger, Irina Fast, Stephanie Fiedler, Stefan Hagemann, Cathy Hohenegger, Thomas Jahns, Silvia Kloster, Stefan Kinne, Gitta Lasslop, Luis Kornblueh, Jochem Marotzke, Daniela Matei, Katharina Meraner, Uwe Mikolajewicz, Kameswarrao Modali, Wolfgang Müller, Julia Nabel, Dirk Notz, Karsten Peters, Robert Pincus, Holger Pohlmann, Julia Pongratz, Sebastian Rast, Hauke Schmidt, Reiner Schnur, Uwe Schulzweida, Katharina Six, Bjorn Stevens, Aiko Voigt, and Erich Roeckner. MPI-M MPIESM1.2-HR model output prepared for CMIP6 CMIP. *Earth System Grid Federation*, 2019. Version 20190710.

[46] Karl-Hermann Wieners, Marco Giorgetta, Johann Jungclaus, Christian Reick, Monika Esch, Matthias Bittner, Stephanie Legutke, Martin Schupfner, Fabian Wachsmann, Veronika Gayler, Helmuth Haak, Philipp de Vrese, Thomas Raddatz, Thorsten Mauritsen, Jin-Song von Storch, Jörg Behrens, Victor Brovkin, Martin Claussen, Traute Crueger, Irina Fast, Stephanie Fiedler, Stefan Hagemann, Cathy Hohenegger, Thomas Jahns, Silvia Kloster, Stefan Kinne, Gitta Lasslop, Luis Kornblueh, Jochem Marotzke, Daniela Matei, Katharina Meraner, Uwe Mikolajewicz, Kameswarrao Modali, Wolfgang Müller, Julia Nabel, Dirk Notz, Karsten Peters, Robert Pincus, Holger Pohlmann, Julia Pongratz, Sebastian Rast, Hauke Schmidt, Reiner Schnur, Uwe Schulzweida, Katharina Six, Bjorn Stevens, Aiko Voigt, and Erich Roeckner. MPI-M MPIESM1.2-LR model output prepared for CMIP6 CMIP. *Earth System Grid Federation*, 2019. Version 20190710.

[47] Oyvind Seland, Mats Bentsen, Dirk Jan Leo Oliviè, Thomas Toniazzo, Ada Gjermundsen, Lise Seland Graff, Jens Boldingh Debernard, Alok Kumar Gupta, Yanchun He, Alf Kirkev, J\"org Schwinger, Jerry Tjiputra, Kjetil Schanke Aas, Ingo Bethke, Yuanchao Fan, Jan Griesfeller, Alf Grini, Chuncheng Guo, Mehmet Ilicak, Inger Helene Hafsahl Karset, Oskar Andreas Landgren, Johan Liakka, Kine Onsum Moseid, Aleksi Nummelin, Clemens Spensberger, Hui Tang, Zhongshi Zhang, Christoph Heinze, Trond Iversen, and Michael Schulz. NCC NorESM2-LM model output prepared for CMIP6 CMIP. *Earth System Grid Federation*, 2019. Version 20190920.

[48] Mats Bentsen, Dirk Jan Leo Oliviè, yvind Seland, Thomas Toniazzo, Ada Gjermundsen, Lise Seland Graff, Jens Boldingh Debernard, Alok Kumar Gupta, Yanchun He, Alf Kirkev, J\"org Schwinger, Jerry Tjiputra, Kjetil Schanke Aas, Ingo Bethke, Yuanchao Fan, Jan Griesfeller, Alf Grini, Chuncheng Guo, Mehmet Ilicak, Inger Helene Hafsahl Karset, Oskar Andreas Landgren, Johan Liakka, Kine Onsum Moseid, Aleksi Nummelin, Clemens Spensberger, Hui Tang, Zhongshi Zhang, Christoph Heinze, Trond Iversen, and Michael Schulz. NCC NorESM2-MM model output prepared for CMIP6 CMIP. *Earth System Grid Federation*, 2019. Version 20191108.

[49] Yongming Tang, Steve Rumbold, Rich Ellis, Douglas Kelley, Jane Mulcahy, Alistair Sellar, Jeremy Walton, and Colin Jones. OHC UKESM1.0-LL model output prepared for CMIP6 CMIP. *Earth System Grid Federation*, 2019. Version 20190627.

[50] Martin Dix, Doahua Bi, Peter Dobrohotoff, Russell Fiedler, Ian Harman, Rachel Law, Chloe Mackallah, Simon Marsland, Siobhan O'Farrell, Harun Rashid, Jhan Srbinovsky, Arnold Sullivan, Claire Trenham, Peter Vohralik, Ian Watterson, Gareth Williams, Matthew Woodhouse, Roger Bodman, Fabio Boeira Dias, Catia Domingues, Nicholas Hannah, Aidan Heerdegen, Abhishek Savita, Scott Wales, Chris Allen, Kelsey Druken, Ben Evans, Clare Richards, Syazwan Mohamed Ridzwan, Dale Roberts, Jon Smillie, Kate Snow, Marshall Ward, and Rui Yang. CSIRO-ARCCSS ACCESS-CM2 model output prepared for CMIP6 DAMIP. *Earth System Grid Federation*, 2019. Version 20191112.

[51] Tilo Ziehn, Matthew Chamberlain, Andrew Lenton, Rachel Law, Roger Bodman, Martin Dix, Yingping Wang, Peter Dobrohotoff, Jhan Srbinovsky, Lauren Stevens, Peter Vohralik, Chloe Mackallah, Arnold Sullivan, Siobhan O'Farrell, and Kelsey Druken. CSIRO ACCESS-ESM1.5 model output prepared for CMIP6 DAMIP. *Earth System Grid Federation*, 2019. Version 20191115.

[52] Neil Cameron Swart, Jason N.S. Cole, Viatcheslav V. Kharin, Mike Lazare, John F. Scinocca, Nathan P. Gillett, James Anstey, Vivek Arora, James R. Christian, Yanjun Jiao, Warren G. Lee, Fouad Majaess, Oleg A. Saenko, Christian Seiler, Clint Seinen, Andrew Shao, Larry Solheim, Knut von Salzen, Duo Yang, Barbara Winter, and Michael Sigmond. CCCma CanESM5 model output prepared for CMIP6 DAMIP. *Earth System Grid Federation*, 2019. Version 20190429.

[53] Aurore Voldoire. CNRM-CERFACS CNRM-CM6-1 model output prepared for CMIP6 DAMIP. *Earth System Grid Federation*, 2019. Version 20180814.

[54] Gareth Jones. MOHC HadGEM3-GC31-LL model output prepared for CMIP6 DAMIP. *Earth System Grid Federation*, 2019.

[55] Olivier Boucher, Sébastien Denvil, Guillaume Levavasseur, Anne Cozic, Arnaud Caubel, Marie-Alice Foujols, Yann Muerdesoif, and Guillaume Gastineau. IPSL IPSL-CM6A-LR model output prepared for CMIP6 DAMIP. *Earth System Grid Federation*, 2018. Version 20190522.